Title: Mutation of *gabra1* is associated with hypermotility and abnormal expression of proteins critical for ion homeostasis and synaptic vesicle transport.

Authors: Nayeli G. Reyes-Nava[1], Isaiah Perez[1], Brian Grajeda[1¶], Igor L. Estevao[1¶], Cameron C. Ellis[1¶], Sourav Roy[1], and Anita M. Quintana[1*].

Affiliations:

[1] Department of Biological Sciences, Border Biomedical Research Center, The University of Texas at El Paso, El Paso, Texas, United States of America

¶These authors contributed equally

*Corresponding author

Email: amquintana8@utep.edu (AQ)

Abstract

Mutation of the *GABRA1* gene is associated with neurodevelopmental defects and epilepsy phenotypes. *GABRA1* encodes for the α1 subunit of the gamma-aminobutyric acid type A receptor ($GABA_AR$), which regulates the fast inhibitory impulses of the nervous system. Multiple model systems have previously been developed to understand the mechanism by which mutations in *GABRA1* cause disease, but these models have produced complex and incongruent data. Thus, additional model systems are required to validate and substantiate previously published results. We investigated the behavioral patterns associated with a non-sense mutation of the zebrafish *gabra1* (*sa43718* allele) gene. The *sa43718* allele has a 90% decrease in total *gabra1* mRNA expression, which is associated with light induced seizure-like behavior. Mutation of *gabra1* was accompanied by increased mRNA expression of *gabra4,* which encodes for the alpha-4 subunit of the $GABA_AR$. Despite increased expression at the RNA level, Gabra4 protein was not increased according to proteomics analysis. Thus, implying that RNA expression patterns of alpha sub-units may not accurately reflect the mechanism underlying seizure. Interestingly, proteomics analysis identified significant enrichment of genes that regulate proton transport, ion homeostasis, vesicle transport, and mitochondrial protein complexes. Collectively, our analysis validates that mutation of *gabra1* results in seizure like phenotypes and provides a blueprint of putative proteins which may mediate these phenotypes *in vivo*.

Introduction

The gamma-aminobutyric acid type A receptor ($GABA_AR$) is a multi-subunit ion channel that mediates inhibitory synapses of the nervous system. The $GABA_AR$ can be composed of unique combinations of any of the following: 6 α subunits, 3 β subunits, 3 γ subunits, and one ε, δ, θ, or π subunits. The most common $GABA_AR$ in mammals consists of 2 α subunits, 2 β subunits, and γ subunit. Each of the subunits is encoded by an independent gene, which are located on different chromosomes. Mutations in many of these subunits have been associated with seizure phenotypes in humans [1] and most recently we used whole exome sequencing to identify a putative heterozygous mutation in the *GABRA1* gene (c.875C>T) associated with seizure phenotypes [2]. *GABRA1* encodes for the α1 subunit of the $GABA_AR$ and to date, over 30 different variants in the *GABRA1* gene have been reported and associated with neurological disorders and neurodevelopmental defects [2]–[11].

Because of its indicated role in neural development, several murine models have been developed to investigate the physiological and behavioral functions of *GABRA1* in mammals, however, the phenotypic outcomes are heterogeneous. For instance, deletion of *Gabra1* or the knock-in of the p.Ala332Asp allele cause behavioral phenotypes that range from tremors/absence-like seizures to the development of myoclonic seizures at postnatal stages [12]–[15]. Noteworthy, these phenotypes are generally strain, age, and sex specific, which makes interpretation of results difficult. Additional zebrafish models have been characterized including a germline mutant and a morpholino mediated transient knockdown. These two studies yielded contrasting results whereby hypermotility

67 was observed in a nonsense mutant of *gabra1* and hypomotility was observed after
68 transient knockdown [2], [16]. Thus, additional complementary models are warranted.

69 In 2016, the zebrafish mutation project was completed by the Wellcome Sanger
70 Institute, where over 40,000 mutant alleles, covering 60% of zebrafish protein-coding
71 genes, were generated [17]. However, only a small number of alleles have been
72 characterized or associated with a specific phenotype. An allele carrying a nonsense
73 mutation in the *gabra1* gene (sa43718) was generated and remains uncharacterized. We
74 hypothesized that a more comprehensive analysis of this allele coud discern the disparate
75 phenotypes observed across other zebrafish approaches. We therefore performed
76 behavioral and molecular analysis of the sa43718 allele.

77 Our results indicate that homozygous *gabra1*$^{sa43718/sa43718}$ larvae show hyperactive
78 locomotion (seizure-like behavior) upon a light stimulus. These behavioral changes are
79 associated with a moderate increase in the expression of *gabra4* transcript, but no change
80 at the level of Gabra4 protein expression. However, differential expression of proteins
81 identified via proteomics approaches revealed abnormal expression of proteins that
82 regulate proton transport, sodium ion homeostasis across the plasma membrane, and the
83 mitochondrial inner membrane protein complex and respiratory chain.

84 Methods

85 Experimental model and animal husbandry

86 The *gabra1*$^{sa43718/+}$ allele (N=10 female fish) was obtained from Sanger Institute through
87 the Zebrafish International Resource Center (ZIRC). Female carriers were outcrossed

88 with wildtype (AB) males to generate independent families of heterozygous male and
89 female carriers. For all experiments, zebrafish larvae were obtained by mating adult
90 heterozygous *gabra1*$^{sa43718/+}$ fish. Collected zebrafish embryos were maintained in E3
91 media (5mM NaCl, 0.17mM KCl, 0.33mM CaCl, 0.33mM MgSO4, 0.05% methylene blue,
92 pH 7.4) at 28°C under 14:10 light: dark cycle. All experimental procedures were
93 performed at 5 days post fertilization (DPF). All animals were maintained and used in
94 accordance with the guidelines from the University of Texas at El Paso Institutional
95 Animal Care and Use Committee (Animal Protocol Number 811869-5). Euthanasia and
96 anesthesia were performed according with the American Veterinary Medical Association
97 (AVMA) guidelines for the euthanasia, 2020 edition.

98 Genotyping

99 Genotyping of the *gabra1*$^{sa4371/sa4371}$ allele was performed by PCR amplification and
100 restriction enzyme digest. Adult fin clips and larval tails were lysed in lysis buffer (30ul)
101 (50mM NaOH) for 5 minutes at 95°C followed by 10 minutes at 4°C. DNA was then
102 neutralized by addition of 500mM Tris-HCL solution (6ul) and used directly for PCR. The
103 fragment of interest (237bp) was amplified by standard PCR at an annealing temperature
104 of 60°C (forward: TTGTGACTCAAAGCCACGAG and reverse:
105 TGAGACGAGAACCATCGTCA). PCR amplicon containing the *sa43718* allele region,
106 was digested with XhoI (NebBiolabs) at 37°C according to manufacturer's guidelines. The
107 mutation present in the *sa43718* inhibits cleavage by XhoI allowing differentiation of
108 wildtype, heterozygous, and homozygous offspring.

109 Behavioral analysis and pentylenetetrazole (PTZ) treatment

110 Behavioral analysis was performed using the ZebraBox (ViewPoint Behavioral
111 Technology, Montreal, Canada). Briefly, embryos were obtained from natural spawning
112 and raised to 5 DPF. Larvae (5 DPF) were individually tracked for swim speed and total
113 distance swam in a 96-well plate. The behavioral analysis consisted of 15 minutes divided
114 into 5-minute intervals of dark/light/dark conditions. All larvae were acclimated to the
115 chamber for 1 hour prior to data acquisition [2]. Data was collected each minute, for a
116 total of 15 minutes and total distance traveled (mm) and speed (mm/s) was calculated as
117 previously described [2]. Experiments were performed in biological duplicates using a
118 minimum of N=30 larvae per trial. Treatment with 10mM pentylenetetrazole (PTZ)
119 (Millipore-Sigma) was performed as previously described [2]. Genotyping of each larvae
120 was performed after behavioral analysis.

121 Quantitative real time PCR (QPCR)

122 Total RNA was isolated from brain homogenates at 5 DPF from wildtype, heterozygous,
123 and homozygous larvae with TRIzol reagent (Invitrogen) according to manufacturer's
124 instructions. RNA was reverse transcribed using the Verso cDNA Synthesis Kit
125 (ThermoFisher Scientific) and total RNA (500ng) was normalized across samples. Gene
126 expression was measured in biological quadruplicates using a pool of at least N=5 larvae
127 per biological replicate. For each individual biological replicate, technical replicates were
128 performed as internal controls. The Applied Biosystems StepOne Plus machine with
129 Applied Biosystems associated software was used for quantitative PCR (qPCR) analysis.
130 Sybr green (ThermoFisher Scientific) based primer pairs were designed for each gene
131 analyzed: *gabra1* (FWD: TCGGGAGTCCAGATTTTGCT, REV:
132 AGAGCGTGTAACCGAAGTCA), g*abra2a* (FWD: GATGGCTACGACAACAGGCT, REV:

133 TGTCCATCGCTGTCGGAAAA), *gabra3* (FWD: GCTGAAGTTCGGGAGCTATG, REV:
134 GGAGCTGATGGTCTCTTTGC), *gabra4* (FWD: GACTGCGATGTACCCCACTT, REV:
135 ATCCAGGTCGGAGTCTGTTG), *gabra5* FWD: CATGACAACACCCAACAAGC, REV:
136 CAGGGCCTTTTGTCCATTTA), *gabra6a* (FWD: TCGCGTACCCATCTTTCTTC, REV:
137 CCCTGAGCTTTTCCAGAGTG), *gabra6b* (FWD: CGGAGGAGTGCTGAAGAAAC, REV:
138 GGGAAAAGGATGCGTGAGTA), *gabrb2* (FWD: CCCGACACCTATTTCCTCAA, REV:
139 TCTCGATCTCCAGTGTGCAG), *gabrg2* (FWD: ACACCCAATAGGATGCTTCG, REV:
140 AGCTGCGCTTCCACTTGTAT). The *rpl13a* gene was used as a reference gene for $2^{\Delta\Delta ct}$
141 quantification. Statistical analysis performed using a *t-test*.

142 Proteomic analysis

143 Protein isolation

144 For protein analysis, total protein was obtained from a pool of whole brain homogenates
145 (n=9) per genotype. Two biological replicates per genotype were collected. Brains were
146 excised and stored for protein isolation in 1X Cell Lysis Buffer (ThermoFisher Scientific)
147 with protease inhibitors cocktail (ThermoFisher Scientific). DNA was isolated from the tail
148 tissue for genotyping and protein was isolated from brain homogenates using manual
149 homogenization. Protein quantification was performed using Precision Red Protein Assay
150 Reagent (Cytoskeleton) according to manufacturer's instructions. Samples were then
151 sent to the Biomolecule Analysis and Omics Unit (BAOU) at The University of Texas El
152 Paso for sample processing and proteomic analysis.

153 Sample preparation for proteomics

154 Proteins were removed from 1X Cell Lysis Buffer by trichloroacetic acid (TCA) protein
155 precipitation. Fifty microliters of 100% TCA (Sigma/Millipore - cat# T6399-5G) was added
156 to 200 µL of sample in 1x Cell Lysis Buffer (Safe Seal microcentrifuge tubes, Sorenson
157 BioScience, cat. No. 12030) and incubated at 4°C for 10 minutes. Total protein ranged
158 from 2 – 5 µg per sample. The precipitated proteins were pelleted by centrifugation for
159 five minutes at 14,000 rcf and the supernatant was discarded. The protein pellet was
160 subsequently washed a total of three times with 200 µL LCMS grade acetone by
161 resuspension and pelleting, the acetone supernatant was discarded each time. Residual
162 acetone was evaporated with a heating block at 95°C for 2 minutes. Samples were stored
163 as a pellet at -80°C until processing for proteomic analysis. Stored pellets were
164 resuspended in 8M Urea prior and subjected to enzymatic tryptic digestion using the
165 PreOmics iST sample preparation kit (catalog no. iST 96x P.O.00027). Briefly,
166 denaturation, alkylation, and reduction were performed with 10 µL LYSE buffer per 1 µg
167 of protein and heated at 80 °C for 20 min while being mixed every 5-minutes. Remaining
168 droplets on the cap were given a brief centrifugation (RT; 300 rcf; 10 sec) and samples
169 were sonicated ten times at 30-second on/off intervals for a total of 5 minutes. Fifty
170 microliters of resuspended DIGEST solution were added to the samples for protein
171 digestion. Sample-filled microtubes were gently vortexed, centrifuged and kept for 90
172 minutes at 37°C in a heating block. Throughout the 90-minute incubation period, samples
173 were gently mixed every 10 minutes. One hundred microliters of STOP solution were
174 added and mixed by pipetting ten times. Samples were then transferred to the cartridge
175 and centrifuged for 1 minute at 3,800 rcf, followed by subsequent 200 µL washes with
176 WASH 1 and WASH 2 solutions according to the manufacturer's instructions. Peptides

177 were eluted in two cycles of 100 µL of ELUTE solution and dried completely in a vacuum
178 evaporator (Savant; Thermo Fisher Scientific) for 90 minutes at 45 °C and 100-mTorr and
179 stored at -80°C until LC-MS/MS acquisition.

180 Liquid chromatography–tandem mass spectrometry (LC-MS/MS)

181 Peptides were resuspended in 4% acetonitrile (ACN) with 0.1% formic acid (FA) at a
182 concentration of 1µg/µL. Peptides were separated by a Dionex Ultimate 3000 UHPLC
183 system (Thermo Scientific) tandem with a Q-Exactive Plus Hybrid Quadrupole-Orbitrap
184 Mass Spectrometer (Thermo Scientific) with Xcalibur software (v. 3.0.63) for data
185 acquisition in positive mode. Peptides were separated on a C18 Acclaim PepMap nanoLC
186 column (75 µm x 50 cm nanoViper, PN 164942, Thermo Fisher Scientific) equilibrated
187 with 4% solvent B (99.9% acetonitrile, 0.1% formic acid) and 96% solvent A (99.9% H2O,
188 0.1% formic acid) kept at 55°C throughout the entire acquisition. One microliter of
189 peptides was loaded onto the column for 15-minutes at a flow rate of 0.5 µL/min and
190 eluted with a multi-step gradient. The flow rate was reduced to 0.3µL/min over the course
191 of 15 min, and solvent B was set to 20% over 100-minutes, then increased to 32% and
192 maintained for 20-minutes before increasing to 95% over 1-minute. The column was
193 washed with 95% solvent B at a flow rate of 0.4 µL/min for 4-minutes to remove/clean any
194 remaining peptides. The column was then re-equilibrated with 4% solvent B at 0.5µL/min
195 until a 180-minutes total runtime. Blank injections were added after each biological
196 replicate, using a 60-minute two sawtooth gradient from 4-95% solvent B, and column re-
197 equilibration at 4% solvent B. The mass spectrometer was set to top10 data-dependent
198 acquisition (DDA), with a scan range of 375 to 1500 m/z and a full MS resolution of
199 70,000; AGC target 3e6. Ions were fragmented with NCE at 27 and collected with an AGC

target of 1e5 at 17,500 resolution, 2 m/z isolation window, maximum IT of 60 ms. Charged exclusion ions were unassigned, 1, 6–8, and >8 charges.

Bioinformatics data analysis

After proteomics analysis, Proteome Discover (PD) 2.5.0.400 (Fisher Scientific) was utilized to identify the proteins from each peptide mixture. The database for Danio rerio was downloaded from UniProtKB; http://www.uniprot.org/ on 21 October 2021 with a database 61,623 sequences. A contaminant dataset was run in parallel composed of trypsin autolysis fragments, keratins, standards found in CRAPome repository and in-house contaminants. PD analysis parameters are as follows: false-discovery rate (FDR) of 1%, HCD MS/MS, fully tryptic peptides only, up to 2 missed cleavages, parent-ion mass of 10 ppm (monoisotopic); fragment mass tolerance of 0.6 Da (in Sequest) and 0.02 Da (in PD 2.1.1.21) (monoisotopic). Two-high confidence peptides per protein were applied for identifications. PD dataset was processed through Scaffold Q+S 5.0.1. Scaffold (Proteome Software, Inc., Portland, OR 97219, USA) was used to probabilistically validate protein identifications derived from MS/MS sequencing results using the X!Tandem and Protein Prophet. Data was transferred to Scaffold LFQ (Proteome Software, Portland, Oregon, USA) which was used to validate and statistically compare protein identifications derived from MS/MS search results. A protein threshold of 95%, peptide threshold of 95%, and a minimum number of 2 peptides were used for protein validation. Normalized weighted spectral counts were used when comparing the samples. To ascertain p-values, Fisher's Exact was run with a control FDR level q * .05 with standard Benjamini-Hochberg correction.

Results

Characterization of the sa43718 allele

The sa43718 allele results in a single base pair substitution in exon 6, which is predicted to result in a premature stop codon (Fig 1A). Exon 6 encodes part of the extracellular domain. We used Sanger sequencing to validate the single base pair substitution shown in Fig 1B (Sibling) &B'(sa43718). Based on the sequence change present in the sa43718 allele, we developed a restriction enzyme based genotyping strategy. The sa43718 allele abolishes an XhoI cleavage site and therefore cannot be cleaved by XhoI in a restriction digest. We performed PCR amplification using primers that flank the substituted nucleotide and used restriction digest to identify wildtype, heterozygous, and homozygous larvae. DNA from wildtype siblings was completely digested as predicted (Fig 1C, lane 2), while DNA from homozygous larvae was completely undigested, and DNA from heterozygous carriers was partially digested (Fig 1C, lane 4 and 3, respectively).

Fig 1. The sa43718 allele carries a single non-sense mutation in the *gabra1* gene. (A) Schematic representation of the *gabra* ^{sa43718} allele. Homozygous individuals of the sa43718 allele (*gabra1*$^{sa43718/sa43718}$) carry a single base pair substitution (C>T) in the *gabra1* gene (ENSDART0000010000), predicted to result in a premature stop. Schematic of exon structure of the *gabra1* gene, not to scale. The sa43718 site is indicated with a red asterisk within exon 6, which encodes the extracellular domain of Gabra1. (B-B') Chromatograph showing confirmation of the sa43718 allele through Sanger sequencing of *gabra1*$^{sa43718/+}$ offspring. (B) Wildtype sibling sequence. (B'): *gabra1*$^{sa43718/sa43718}$ sequence. (C) Restriction enzyme digest gel showing digestion of PCR fragments of genomic *gabra1.* The sa43718 allele abolishes the XhoI recognition site. Therefore, digestion of homozygous (sa43718/sa43718) sample results in an uncut fragment, whereas digestion of wildtype (sibling) sample results in a fully digested fragment. LDR: 1kb plus ladder. (D) The offspring of *gabra1*$^{sa43718/+}$ fish was genotyped by tail-clipping at 3 days post fertilization (DPF). Larvae were raised separately according to their genotypes (sibling n=11,

248 sa43718/+ n=13, sa43718/sa43718 n=14), and their survival was monitored until day 22.
249 Premature death of homozygous carriers of the sa43718 allele (sa43718/sa43718*)* was observed
250 starting at day 7 post fertilization, when compared to the wildtype (sibling) and heterozygous
251 (sa43718*/+)* siblings.

252

253 Homozygous mutation in zebrafish *gabra1* has been associated with early lethality.
254 Consequently, we performed a survival assay and monitored the survival for 22 DPF. We
255 observed a 50% survival rate in wildtype and heterozygous siblings, but all homozygous
256 carriers of the sa43718 allele died by 22 DPF (Fig 1D). The remaining heterozygous
257 individuals survived into adulthood.

258 Expression of $GABA_A$ receptor subunits in the sa43718 allele.

259 Based on our previous studies, we hypothesized that the expression of other $GABA_AR$
260 receptor subunits were disrupted in the sa43718 allele. We first measured the expression
261 of β2 and γ2 subunits, as these are present in the most common form of the $GABA_AR$
262 receptor, alongside α1. We validated that the sa43718 allele reduced the expression of
263 *gabra1* (Fig 2A), but that decrease was not associated with decreased expression of β2
264 and γ2 transcripts (Fig 2A). We therefore hypothesized that these subunits were in
265 complex with other α subunits to compensate for the loss of α1. We measured the
266 expression of α2-6 (including 6a and 6b due to gene duplication). We observed a mild
267 increase in *gabra4* (α4) gene expression, which was statistically significant (Fig 2B).
268 However, we did not detect a significant difference in any other α subunit (Fig 2B).

269 **Fig 2. Non-sense mutation of *gabra1* results in decreased expression of *gabra1*.** (A)
270 Quantitative real time PCR (qPCR) analyzing the relative mRNA expression of major $GABA_AR$
271 subunits, α1 (*gabra1),* β2 *(gabrb2)* and, γ2 (*gabrg2)* at 5 days post fertilization (DPF). n≥5 larvae

272 per group with five biological replicates. Error bars represent the standard error of the mean of
273 biological replicates. *p=1.00511E-07. (B) Relative expression of genes encoding for alpha type
274 subunits, *gabra2a* (α2), *gabra3* (α3), *gabra4* (α4), *gabra5* (α5), *gabra6a* (α6a), and *gabra6b* (α6b),
275 was analyzed in wildtype siblings (sibling) and homozygous (sa43718/sa43718) mutants. n≥5
276 larvae per group in four independent biological replicates. Error bars represent the standard error
277 of the mean. *p=0.002884.

278

279 Mutation of *gabra1* results in seizure-like behavior

280 We have previously reported hypoactivity at 5 DPF upon knockdown of *gabra1* [2]. In
281 contrast, seizure-like behavior at juvenile stages has been reported in a zebrafish model
282 of *gabra1* loss of function [16]. To begin to rectify these differences, we monitored
283 swimming behavior after a light stimulus, which has been shown to induce seizure like
284 behavior in a previous allele of *gabra1* mutation. We measured baseline activity for a
285 period of 5 minutes in the dark after a 1-hour acclimation period. During this time, we did
286 not observe any differences in baseline swimming patterns according to total distance
287 swam (mm) or swim speed (mm/s) in the sa43718 allele (Fig 3A&A'). However, after light
288 stimulus, we detected a marked increase in swim speed in the sa43718 allele (Fig 3A&A').
289 Swim patterns were increased in mutant larvae during the entire light stimulus (Fig
290 3C&C'). Importantly, increased speed (velocity) was associated with rapid circling
291 behavior, hyperactivity burst, and whirlpool behavior (Fig 3B) indicative of a seizure-like
292 behavior as defined by the zebrafish behavioral glossary [18]. Because we did not
293 observe behavioral changes in heterozygous carriers in comparison to wildtype siblings,
294 all data shown here are from sibling wildtype or homozygous carriers of the sa43718
295 allele.

296 **Fig 3. *gabra1*$^{sa43718/sa43718}$ larvae undergo seizure-like behavior upon light stimuli.** (A & A')
297 Behavioral analysis of sa43718 allele and wildtype siblings at 5 days post fertilization. (A) Swim
298 speed (mm/s) over 15 minutes (900 seconds) in dark-light-dark transitions [5 minutes (0-300
299 seconds) in the dark, 5 minutes (300-600 seconds) in the light, and 5 minutes (600-900 seconds)
300 in the dark) was analyzed using the Zebrabox technology. Data was collected every minute (60
301 seconds). *gabra1*$^{sa43718/sa43718}$ larvae undergo hyperlocomotion upon light stimuli when compared
302 to their wildtype siblings (Sibling). *$p<0.05$. (A') Total distance swam over 15 minutes in dark-light-
303 dark transitions. Homozygous carriers (sa43718/sa43718) larvae showed increased distance
304 swam across the light phase, showing a statistically significant increase at seconds 480-540
305 (minute 9), when compared to their wildtype counterparts (sibling). *gabra1*$^{sa43718/sa43718}$ larvae then
306 show decreased distance swam under dark conditions (600-660s) when compared to their
307 wildtype siblings (sibling) *$p<0.05$. (B) Representative images of swimming track of a single
308 larvae, representing each genotype, generated from the Viewpoint Zebralab Tracking software in
309 dark (180-240s), light (480-540s), and dark (600-660s) conditions. Green lines indicate
310 movements between 4-8mm/s and red lines indicate burst movements (>8mm/s). (C) Average
311 total speed representing overall behavioral responses in dark-light-dark conditions of *gabra1*
312 wildtype (sibling) and homozygous (sa43718/sa43718) larvae. Homozygous carriers
313 (sa43718/sa43718) showed increased average swim speed in light conditions when compared to
314 their wildtype (sibling) counterparts. (C') Average total distance swam representing overall
315 behavioral responses in dark-light-dark conditions of *gabra1* wildtype (sibling) and homozygous
316 (sa43718/sa43718) larvae. No statistically significant changes were observed in homozygous
317 larvae (sa43718/sa43718) when compared to their wildtype siblings for average distance
318 measurements. All behavioral analysis was performed using a minimum of 30 larvae per
319 biological replicate, over three independent biological replicates. Representative analysis of a
320 single biological replicate is shown here. Sibling (n=13) and *gabra1*$^{sa43718/sa43718}$ (n=26).

321

322 *Gabra1 sa43718* response to PTZ

323 We have previously demonstrated that reduced *gabra1* expression does not prohibit
324 receptor responses to pentylenetetrazole (PTZ), a $GABA_AR$ antagonist [2]. We also
325 observed increased expression of *gabra4* and therefore, we sought to understand if the

326 sa43718 allele would respond to PTZ, which may indicate the presence of a functional
327 receptor. As shown in Fig 4A, treatment with PTZ induces increased swimming distance
328 and speed in wildtype larvae. Within the first five minutes post treatment, in dark
329 conditions, wildtype larvae exhibit an average 2-fold change in total distance swam and
330 a 1.54-fold change in swim speed. However, the sa43718 allele had a slightly reduced
331 response to PTZ in the dark accounting for a 1.7-fold change in total distance swam and
332 a 1.2-fold change in swim speed in dark conditions (minutes 1-5) (Fig 4C-D). We
333 continued to monitor the speed and distance swam after light stimulus in PTZ treated
334 larvae. After light stimulus, wildtype sibling larvae showed a 1.5-fold change in average
335 swim speed and a 2.5-fold change in average total distance swam (Fig 4C-D). Whereby,
336 the sa43718 allele exhibited a 1.4-fold change in average swim speed and 1.7-fold
337 change in average distance swam in response to PTZ treatment (Fig 4C-D). The reduced
338 response to PTZ treatment by the sa43718 allele was statistically significant in dark
339 conditions for speed (p=0.03) and distance (p=0.002).

340 **Fig 4. Locomotion response to pentylenetetrazole (PTZ) in the sa43718 allele.** (A-B).
341 Behavioral responses of the sa43718 allele at 5 days post fertilization (DPF) were analyzed using
342 the Zebrabox. (A) Comparison of wildtype sibling (Sibling) larvae response to treatment with 10uM
343 PTZ (10uM PTZ) or no treatment (NO PTZ) at 5 days post fertilization. NO PTZ n=18, 10uM PTZ
344 n=16. *p<0.05 (B) Comparison of homozygous carriers (sa43718/sa43718) response to treatment
345 with 10uM PTZ (10uM PTZ) or no treatment (NO PTZ) at 5 days post fertilization. NO PTZ n=13,
346 10uM PTZ n=14. *p<0.05. Swim speed (mm/s) was analyzed using the distance swam and
347 swimming duration data generated by ViewPoint software. Larvae were monitored for 5 minutes
348 in the dark (0-300 s), 5 minutes in the light (300-600 s), and 5 minutes in the dark (600-900 s).
349 Data was collected every minute (60 s). Error bars represent the standard error of the mean. (C)
350 Average fold change (total distance) response to treatment with PTZ in dark (0-300s) and light
351 (300-600s) conditions by wildtype (sibling) and sa43718/sa43718 mutants. *p=0.002. (D) Average
352 fold change (swim speed) response to treatment with PTZ in dark (0-300s) and light (300-600s)

353 conditions by wildtype (sibling) and sa43718/sa43718 mutants. *p=0.03. Error bars represent
354 standard deviation in C-D.

355

356 Proteomic analysis identifies differentially expressed
357 proteins (DEPs) in the sa43718 allele.

358 To begin to understand the underlying molecular mechanisms by which seizure
359 phenotypes occurred, we performed proteomics analysis. We isolated protein from whole
360 brain homogenates isolated from wildtype and homozygous larvae. A total of 3500
361 proteins were identified in the wildtype sibling brain homogenate, 3511 were identified in
362 heterozygous animals, and 3552 were identified in the homozygous carriers of the
363 sa43718 allele. A complete list of identified proteins is in S1 file. From these proteins, we
364 identified a total of 173 DEPs in homozygous mutants relative to wildtype clutch mates.
365 Of these 81 were up-regulated and 93 were down-regulated. These DEPs are
366 summarized in the volcano plot shown inf Fig 5A. A complete list of DEPs can be found
367 in file S2. DEPs of interest include Synaptotagmin, Complexin 4a, Dynactin subunit 1,
368 Dynamin GTPase, Secretogranin II, and a Vat1 homolog. Each of these proteins has a
369 function in synaptic fusion, transport, exocytosis, endocytosis, or direct interactions with
370 small synaptic vesicles. Interestingly, we also noted a significant number of DEPs
371 involved in microtubule growth, microtubule binding, vesicle recycling, retrograde
372 transport along microtubules, or microtubule folding. These include microtubule
373 associated protein, RP/EB family member 3b, Dynactin subunit 1, Dynamin GTPase, and
374 Tubulin-specific chaperone A.

375 We further annotated DEPs by biological process (Fig 5B), molecular function (Fig
376 5C), and cellular process (Fig 5D). According to biological process, DEPs were clustered
377 in Gene Ontology (GO) groups associated with proton transport including sodium and
378 potassium export across the plasma membrane. Some examples of DEPs in this category
379 include Slc82b, Atp1a1b, Atp1b3a, and Atp1a1a.3. All these DEPs are important for
380 sodium and potassium homeostasis consistent with GO analysis. GO analysis by
381 molecular function also indicated molecular carrier activity and active transport
382 mechanisms, consistent with the GO analysis according to biological process. GO
383 analysis by cellular process indicated DEPs in the respiratory chain, mitochondrial protein
384 containing complexes, the cytoskeleton, proton transport, and exocytosis. These data
385 collectively indicate mitochondrial transport, synaptic vesicle regulation, and proton
386 homeostasis are dysregulated after mutation of *Gabra1*.

387 **Fig 5. Proteomic analysis of sa43718 allele carriers.** (A) Volcano plot of differentially
388 expressed proteins between wildtype siblings and homozygous (sa43718/sa43718)
389 larvae. Volcano plot show –log10 P-values from the normalized proteomics data exported
390 from Scaffold LFQ versus log2foldchange (FC) across each contrast. Thresholds set were
391 p-value ≤ 0.05 and Log2FC ≤ -1.5 or ≥ 1.5. (B-D) Gene Ontology terms enriched by
392 proteins with significant expression (p-value <0.05) between wildtype sibling and sa43718
393 homozygous mutant larvae at 5 days post fertilization. Terms are separated by (B)
394 Biological Process, (C) Molecular Function, (D) Cellular Process.

395

396 Discussion

397 The $GABA_AR$ has previously been associated with seizure and epileptic
398 phenotypes [1], [9], [15]. In support of this notion, we reported a heterozygous missense

399 mutation in humans that is associated with a seizure phenotyes [2]. Multiple model
400 systems have been developed to study early *GABRA1* function. These include mouse
401 and zebrafish models. Survival of homozygous knockouts in mice and zebrafish is
402 compromised [12], [16]. Due to external fertilization and early juvenile survival of
403 homozygous mutants, zebrafish provide a window of opportunity to analyze
404 developmental and juvenile onset of seizures [19]–[24]. However, in previous studies
405 germline nonsense mutation of zebrafish *gabra1* and morpholino mediated knockdown of
406 *gabra1* demonstrated different behavioral phenotypes after a light stimulus [2], [16]. Here
407 we characterized the phenotypes of a novel allele, known as the sa43718 allele. The
408 sa43718 allele is a single base pair change in exon 6, which results in a premature stop
409 codon and leads to a greater than 90% decrease in *gabra1* expression, indicating the
410 possibility of nonsense mediated decay of the mutated transcript. The sa43718 allele
411 reduces viability and homozygous mutants die by 22 DPF. This is consistent with the
412 viability of other zebrafish [16] and mouse models [13].

413 We observed seizure like (hypermotility, whirlpool behavior) behavior upon light
414 stimuli in the sa43718 allele. These data are supported by previously published works,
415 which established seizure like behavior at the juvenile stage in an additional zebrafish
416 germline mutant [16]. Similar results have also been documented in mouse models of
417 *Gabra1* mutation, although these data are sex and strain specific [12]–[14]. In our
418 experiments, the zebrafish larvae have not yet determined sex and therefore, sex is not
419 a variable considered in our experiments. Hyperactivity and seizure like behavior in the
420 sa43718 allele contrasts with our previous study using morpholino mediated knockdown
421 [2]. There are several reasons for these differences. For example, we validated an

422 approximate 50% knockdown of *gabra1* in morphants, which would most likely reflect a
423 haploinsufficency or dosage effect. In addition, *gabra1* morphants demonstrated with
424 decreased expression of other $GABA_A$ receptor subunits. We did not observe statistically
425 significant differences in other subunits, except for the *gabra4* subunit. However, this was
426 only at the mRNA level, as proteomics did not reveal differences in the Gabra4 protein
427 level in the sa43718 allele.

428 Given the normal expression of other $GABA_AR$ subunits, it is not surprising that
429 sa43718 larvae responded to PTZ treatment. Mutant larvae were capable of a response
430 to 10uM PTZ, which has been shown to induce seizures in zebrafish [25], [26]. These
431 data are consistent with our previous work, which demonstrated that *gabra1* knockdown
432 did not affect response to PTZ [2]. Additionally, Samarut and colleagues demonstrated
433 that the overall brain morphology of *gabra1* mutant brains was normal. Despite an
434 overwhelming normal morphology, Samarut and colleagues did show 460 differentially
435 expressed genes in *gabra1* mutant brains. Of these genes, 3 $GABA_AR$ subunits, in
436 addition to *gabra1*, were down regulated [16]. We observed increased expression of
437 *gabra4* here and in a previous study we found *gabra6* to be up regulated at the
438 transcriptional level after morpholino mediated knockdown [2]. These data are partially
439 supported by murine studies that show abnormal expression of receptor subunits.
440 Although data from murine studies are mutant, strain, and gender specific [27], [28]. We
441 performed proteomics analysis to determine if these changes translate to differential
442 expression of proteins. We did not identify a single $GABA_AR$ subunit differentially
443 expressed in the sa43718 allele at the protein level. These data are consistent with the
444 ability of *gabra1* mutants to respond to PTZ, indicating the presence of a receptor.

445 Our proteomics analysis identified proteins with functions in synaptic vesicle
446 transport, microtubule organization/growth, mitochondrial function, and regulation of
447 potassium and sodium homeostasis as differentially expressed. A subset of these data
448 are consistent with data from Samarut and colleagues, who noted decreased expression
449 of kinesin motor proteins [16]. However, the functional significance of differential
450 expression of transcripts is unclear because we did not validate up-regulation of Gabra4
451 protein despite increased transcript. Thus, there are some differences from our protein
452 data relative to previous results. For example, we did not identify statistically significant
453 changes in neuroligins 2 and 4, nor other $GABA_A$ subunits. We cannot rule out differential
454 expression of these proteins, however, in our analysis we did not find significant changes
455 in protein expression. Of note, we identified abnormal expression of synaptotagmin,
456 secretogranin II, and synapsin IIb; all of which are important for synaptic vesicle release
457 at the presynaptic membrane. Synapsin I was also downregulated and has been
458 associated with epileptic phenotypes [29]–[32]. Furthermore, we identified
459 downregulation of proteins implicated in mitochondrial complex I deficiency, including
460 NADH:ubiquinone oxidoreductase core subunit S2 and NADH:ubiquinone
461 oxidoreductase core subunit A10. Remarkably, mutations in the genes encoding these
462 proteins are associated with Leigh syndrome, one of the most common mitochondrial
463 diseases, in which epilepsy is a primary phenotype [33], [34]. Interestingly, mutation of
464 *GABRA1* in humans have been prematurely diagnosed as a primary mitochondrial
465 disorder prior to exome sequencing [23]. Interestingly, none of the DEPs discovered
466 inhibited the response to PTZ, a $GABA_AR$ agonist, suggesting that a residual receptor is
467 present. Nonetheless, our proteomics data implicates neurotransmitter release, vesicle

468 transport, microtubule structure, proton homeostasis, and regulation of mitochondrial
469 proteins as putative underlying mechanisms resulting in seizure-like phenotypes after
470 mutation of *gabra1*.

471 Here we have characterized an additional germline mutant of the zebrafish *gabra1*
472 gene. We observed early lethality, seizure-like hypermotility after light stimuli, and
473 abnormal expression of proteins involved in vesicle transport, synaptic vesicle release,
474 exocytosis, and endocytosis. Our data support the hypermotility and expression patterns
475 previously described in a secondary zebrafish germline mutant [16]. Collectively, these
476 data suggest that models derived from germline mutation of *gabra1* rather than transient
477 knockdown are more physiologically relevant to human disease.

478

479 Acknowledgements

480 The authors would like to thank the members of the Quintana Lab, past and present, for
481 discussions, animal care, genotyping, and general laboratory maintenance. A special
482 thank you to Pamela Rodriguez and Carla Canales for their efforts in the laboratory and
483 their explicit help with genotyping embryos related to this manuscript. The work provided
484 herein could not be completed without the support of The University of Texas El Paso
485 core facilities and Border Biomedical Research Center (BBRC). We graciously thank Dr.
486 Robert Kirken, Dr. Igor C. Almeida, and Dr. Renato Aguilera for their directorships of the
487 BBRC and core facilities.

488

489 # References

490 1. Macdonald RL, Gallagher MJ, Feng HJ, Kang J. GABAA receptor epilepsy
491 mutations. Biochem Pharmacol. 2004 Oct;68(8):1497–506.
492 2. Reyes-Nava NG, Yu HC, Coughlin CR, Shaikh TH, Quintana AM. Abnormal
493 expression of GABAA receptor subunits and hypomotility upon loss of gabra1 in
494 zebrafish. Biol Open [Internet]. 2020 Apr 15 [cited 2020 Apr 14];9(4). Available from:
495 https://bio.biologists.org/content/9/4/bio051367
496 3. Steudle F, Rehman S, Bampali K, Simeone X, Rona Z, Hauser E, et al. A novel de
497 novo variant of GABRA1 causes increased sensitivity for GABA in vitro. Sci Rep.
498 2020 Feb 11;10(1):2379.
499 4. Choi YJ, Lee SY, Yang KS, Park JY, Yoon SZ, Yoon SM. Polymorphism rs4263535
500 in GABRA1 intron 4 was related to deeper sedation by intravenous midazolam. J Int
501 Med Res. 2015 Oct;43(5):686–98.
502 5. Cossette P, Liu L, Brisebois K, Dong H, Lortie A, Vanasse M, et al. Mutation of
503 *GABRA1* in an autosomal dominant form of juvenile myoclonic epilepsy. Nat Genet.
504 2002 Jun;31(2):184–9.
505 6. Farnaes L, Nahas SA, Chowdhury S, Nelson J, Batalov S, Dimmock DM, et al. Rapid
506 whole-genome sequencing identifies a novelGABRA1variant associated with West
507 syndrome. Cold Spring Harb Mol Case Stud. 2017 Sep;3(5).
508 7. Kodera H, Ohba C, Kato M, Maeda T, Araki K, Tajima D, et al. De novo GABRA1
509 mutations in Ohtahara and West syndromes. Epilepsia. 2016 Apr;57(4):566–73.

510 8. Epi4K Consortium, Epilepsy Phenome/Genome Project, Allen AS, Berkovic SF,
511 Cossette P, Delanty N, et al. De novo mutations in epileptic encephalopathies.
512 Nature. 2013 Sep 12;501(7466):217–21.
513 9. Hirose S. Chapter 3 - Mutant GABAA receptor subunits in genetic (idiopathic)
514 epilepsy. In: Steinlein OK, editor. Progress in Brain Research [Internet]. Elsevier;
515 2014 [cited 2018 Jul 30]. p. 55–85. (Genetics of Epilepsy; vol. 213). Available from:
516 http://www.sciencedirect.com/science/article/pii/B978044463326200003X
517 10. Johannesen K, Marini C, Pfeffer S, Møller RS, Dorn T, Niturad CE, et al. Phenotypic
518 spectrum of GABRA1: From generalized epilepsies to severe epileptic
519 encephalopathies. Neurology. 2016 13;87(11):1140–51.
520 11. Maillard PY, Baer S, Schaefer É, Desnous B, Villeneuve N, Lépine A, et al. Molecular
521 and clinical descriptions of patients with GABAA receptor gene variants (GABRA1,
522 GABRB2, GABRB3, GABRG2): A cohort study, review of literature, and genotype–
523 phenotype correlation. Epilepsia. 2022;63(10):2519–33.
524 12. Ye GL, Baker KB, Mason SM, Zhang W, Kirkpatrick L, Lanthorn TH, et al. GABAA
525 Receptor α1 Subunit (Gabra1) Knockout Mice: Review and New Results. In: Kalueff
526 AV, Bergner CL, editors. Transgenic and Mutant Tools to Model Brain Disorders
527 [Internet]. Totowa, NJ: Humana Press; 2010 [cited 2020 Apr 9]. p. 65–90.
528 (Neuromethods). Available from: https://doi.org/10.1007/978-1-60761-474-6_4
529 13. Arain FM, Boyd KL, Gallagher MJ. Decreased viability and absence-like epilepsy in
530 mice lacking or deficient in the GABAA receptor α1 subunit. Epilepsia. 2012
531 Aug;53(8):e161-165.

532 14. Arain F, Zhou C, Ding L, Zaidi S, Gallagher MJ. The Developmental Evolution of the
533 Seizure Phenotype and Cortical Inhibition in Mouse Models of Juvenile Myoclonic
534 Epilepsy. Neurobiol Dis. 2015 Oct;82:164–75.
535 15. Maljevic S, Møller RS, Reid CA, Pérez-Palma E, Lal D, May P, et al. Spectrum of
536 GABAA receptor variants in epilepsy: Curr Opin Neurol. 2019 Apr;32(2):183–90.
537 16. Samarut É, Swaminathan A, Riché R, Liao M, Hassan-Abdi R, Renault S, et al. γ-
538 Aminobutyric acid receptor alpha 1 subunit loss of function causes genetic
539 generalized epilepsy by impairing inhibitory network neurodevelopment. Epilepsia.
540 2018 Nov 1;59(11):2061–74.
541 17. ZMP | Busch Lab [Internet]. [cited 2022 Oct 24]. Available from:
542 https://zmp.buschlab.org/
543 18. Kalueff AV, Gebhardt M, Stewart AM, Cachat JM, Brimmer M, Chawla JS, et al.
544 Towards a comprehensive catalog of zebrafish behavior 1.0 and beyond. Zebrafish.
545 2013 Mar;10(1):70–86.
546 19. Canzian J, Müller TE, Franscescon F, Michelotti P, Fontana BD, Costa FV, et al.
547 Modeling psychiatric comorbid symptoms of epileptic seizures in zebrafish. J
548 Psychiatr Res. 2019 Dec 1;119:14–22.
549 20. Grone BP, Baraban SC. Animal models in epilepsy research: legacies and new
550 directions. Nat Neurosci. 2015 Mar;18(3):339–43.
551 21. Yaksi E, Jamali A, Diaz Verdugo C, Jurisch-Yaksi N. Past, present and future of
552 zebrafish in epilepsy research. FEBS J. 2021;288(24):7243–55.

553 22. Stewart AM, Desmond D, Kyzar E, Gaikwad S, Roth A, Riehl R, et al. Perspectives
554 of zebrafish models of epilepsy: what, how and where next? Brain Res Bull. 2012
555 Feb 10;87(2–3):135–43.
556 23. Reyes-Nava NG. Zebrafish: A Comprehensive Model to Understand the
557 Mechanisms Underlying Neurodevelopmental Disorders. In: Costa, Andres., Villalba,
558 Eugenio., editors. Horizons in Neuroscience Research. Nova Biomedical; 2018.
559 24. Gawel K, Langlois M, Martins T, van der Ent W, Tiraboschi E, Jacmin M, et al.
560 Seizing the moment: Zebrafish epilepsy models. Neurosci Biobehav Rev. 2020 Sep
561 1;116:1–20.
562 25. Baraban SC, Taylor MR, Castro PA, Baier H. Pentylenetetrazole induced changes
563 in zebrafish behavior, neural activity and c-fos expression. Neuroscience. 2005 Jan
564 1;131(3):759–68.
565 26. Afrikanova T, Serruys ASK, Buenafe OEM, Clinckers R, Smolders I, Witte PAM de,
566 et al. Validation of the Zebrafish Pentylenetetrazol Seizure Model: Locomotor versus
567 Electrographic Responses to Antiepileptic Drugs. PLOS ONE. 2013 Jan
568 14;8(1):e54166.
569 27. Zhou C, Huang Z, Ding L, Deel ME, Arain FM, Murray CR, et al. Altered cortical
570 GABAA receptor composition, physiology, and endocytosis in a mouse model of a
571 human genetic absence epilepsy syndrome. J Biol Chem. 2013 Jul
572 19;288(29):21458–72.
573 28. Zhou C, Ding L, Deel ME, Ferrick EA, Emeson RB, Gallagher MJ. Altered
574 Intrathalamic GABAA Neurotransmission in a Mouse Model of a Human Genetic
575 Absence Epilepsy Syndrome. Neurobiol Dis. 2015 Jan;73:407–17.

576 29. Fassio A, Raimondi A, Lignani G, Benfenati F, Baldelli P. Synapsins: From synapse
577 to network hyperexcitability and epilepsy. Semin Cell Dev Biol. 2011 Jun
578 1;22(4):408–15.
579 30. Garcia CC. Identification of a mutation in synapsin I, a synaptic vesicle protein, in a
580 family with epilepsy. J Med Genet. 2004 Mar 1;41(3):183–6.
581 31. Giannandrea M, Guarnieri FC, Gehring NH, Monzani E, Benfenati F, Kulozik AE, et
582 al. Nonsense-Mediated mRNA Decay and Loss-of-Function of the Protein Underlie
583 the X-Linked Epilepsy Associated with the W356× Mutation in Synapsin I. PLOS
584 ONE. 2013 Jun 20;8(6):e67724.
585 32. Barbieri R, Contestabile A, Ciardo MG, Forte N, Marte A, Baldelli P, et al. Synapsin
586 I and Synapsin II regulate neurogenesis in the dentate gyrus of adult mice.
587 Oncotarget. 2018 Apr 10;9(27):18760–74.
588 33. Lopriore P, Gomes F, Montano V, Siciliano G, Mancuso M. Mitochondrial Epilepsy,
589 a Challenge for Neurologists. Int J Mol Sci. 2022 Oct 30;23(21):13216.
590 34. Schubert Baldo M, Vilarinho L. Molecular basis of Leigh syndrome: a current look.
591 Orphanet J Rare Dis. 2020 Jan 29;15(1):31.

592

593 # Supporting information

594 **S1 File. Complete list of identified proteins.**

595 **S2 File. Complete list of differentially expressed proteins.**

596

Funding

Partial funding for this project was provided by K01NS099153 to AMQ, R03DE029517 to AMQ, NIMHD grant No 5U54MD007592 to University of Texas El Paso, RISE program grant No R25GM069621-11 from NIGMS, and NIGMS linked awards RL5GM118969, TL4GM118971, and UL1GM118970 to the University of Texas El Paso. NGR was partially supported by Keelung-Hong Fellowship. We thank the Biomolecule Analysis and Omics Unit (BAOU) at BBRC/UTEP, for the full access to the nanoUHPLC-ESI-Q Exactive Plus orbitrap MS system used in this study. AMQ was provided pilot grant funds that partially funded this award as a component of the 5U54MD007592 award. The content is solely the responsibility of the authors and does not represent the official views of the funding agencies.

Author contributions

NGR performed experiments, provided experimental conceptualization, wrote aspects of the manuscript, performed zebrafish care and maintenance, supervised trainees that provided input/data analysis or acquisition. AMQ performed data analysis, wrote portions of the manuscript, obtained funding, provided mentorship to NGR, and performed data analysis. IP performed survival analysis and produced graphs related to survival. BG, ILE, and CCE performed mass spectrometry, protein isolation, and data analysis for proteomics. SR supervised and provided additional correction for BG data analysis.

Data availability

All data and reagents are available upon request from the corresponding author.

Competing interests

Authors declare no competing or financial interests.

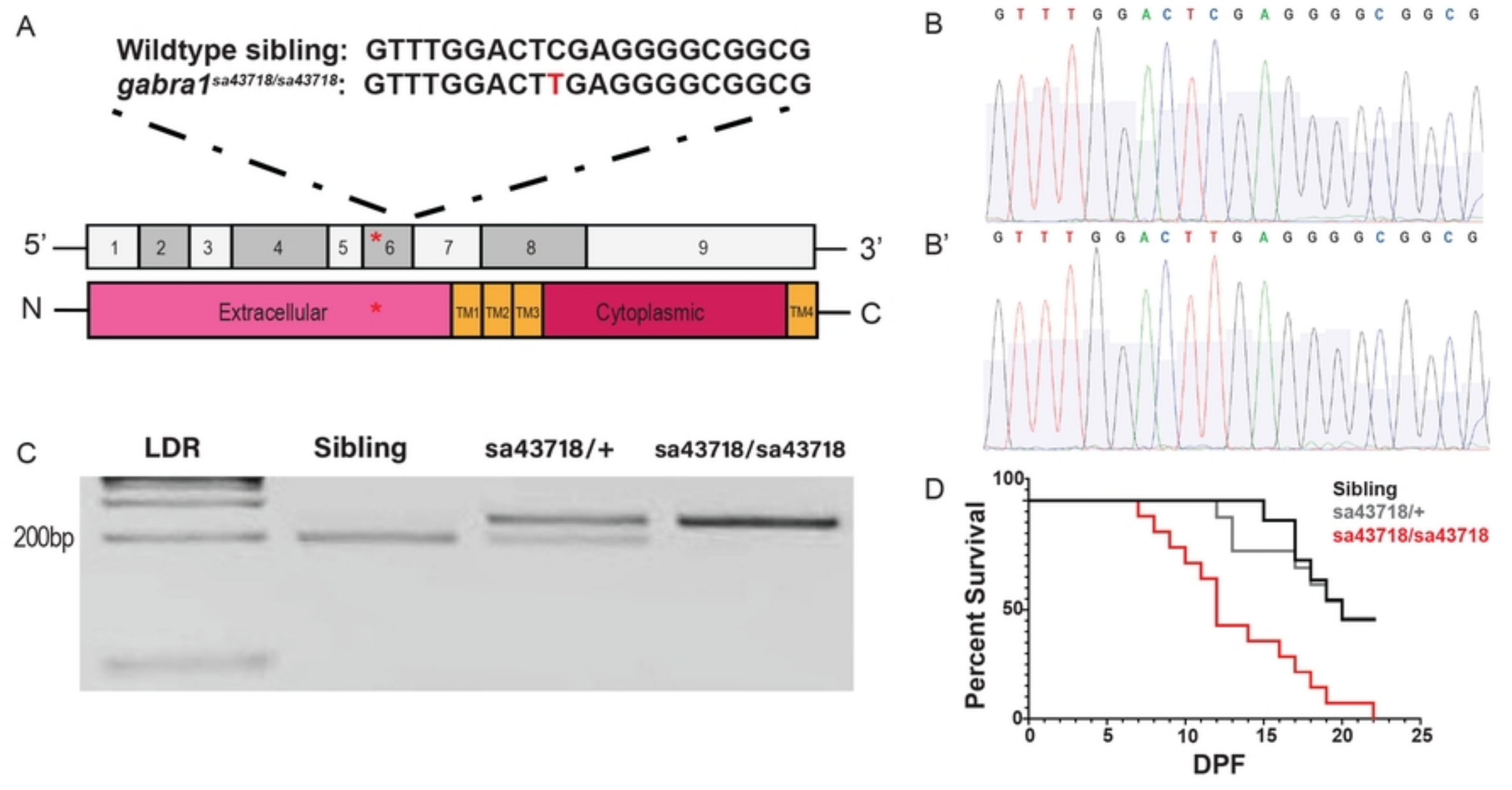
A
Wildtype sibling: GTTTGGACTCGAGGGGCGGCG
gabra1sa43718/sa43718: GTTTGGACTTGAGGGGCGGCG
5'
1
2
3
4
5
6
7
8
9
3'
N
Extracellular
TM1
TM2
TM3
Cytoplasmic
TM4
C
B
B'
C
LDR
Sibling
sa43718/+
sa43718/sa43718
200bp
D
Percent Survival
DPF
Sibling
sa43718/+
sa43718/sa43718

Figure 1

A

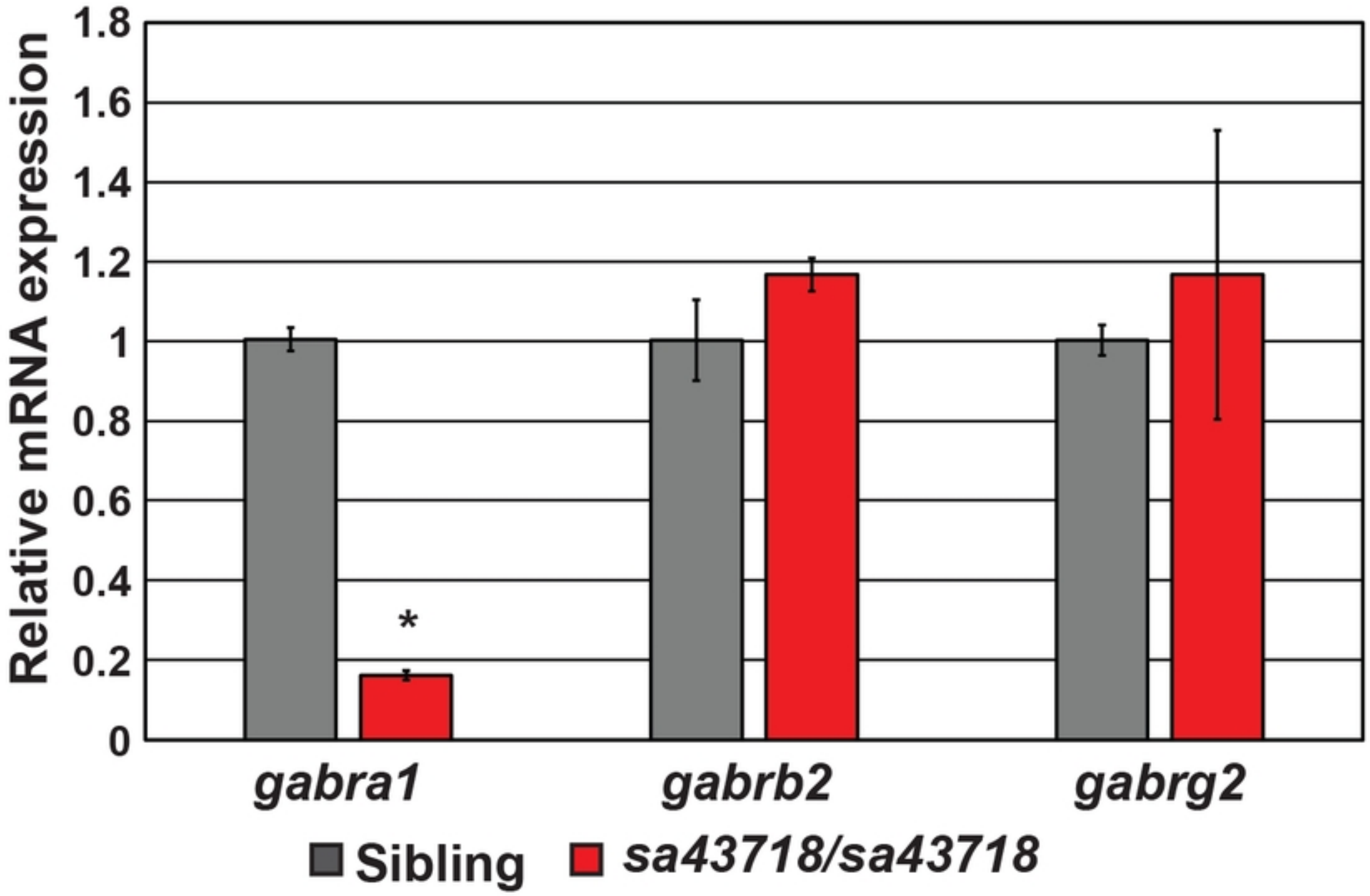
Relative mRNA expression
1.8
1.6
1.4
1.2
1
0.8
0.6
0.4
0.2
0
*
gabra1
gabrb2
gabrg2
Sibling
sa43718/sa43718

B

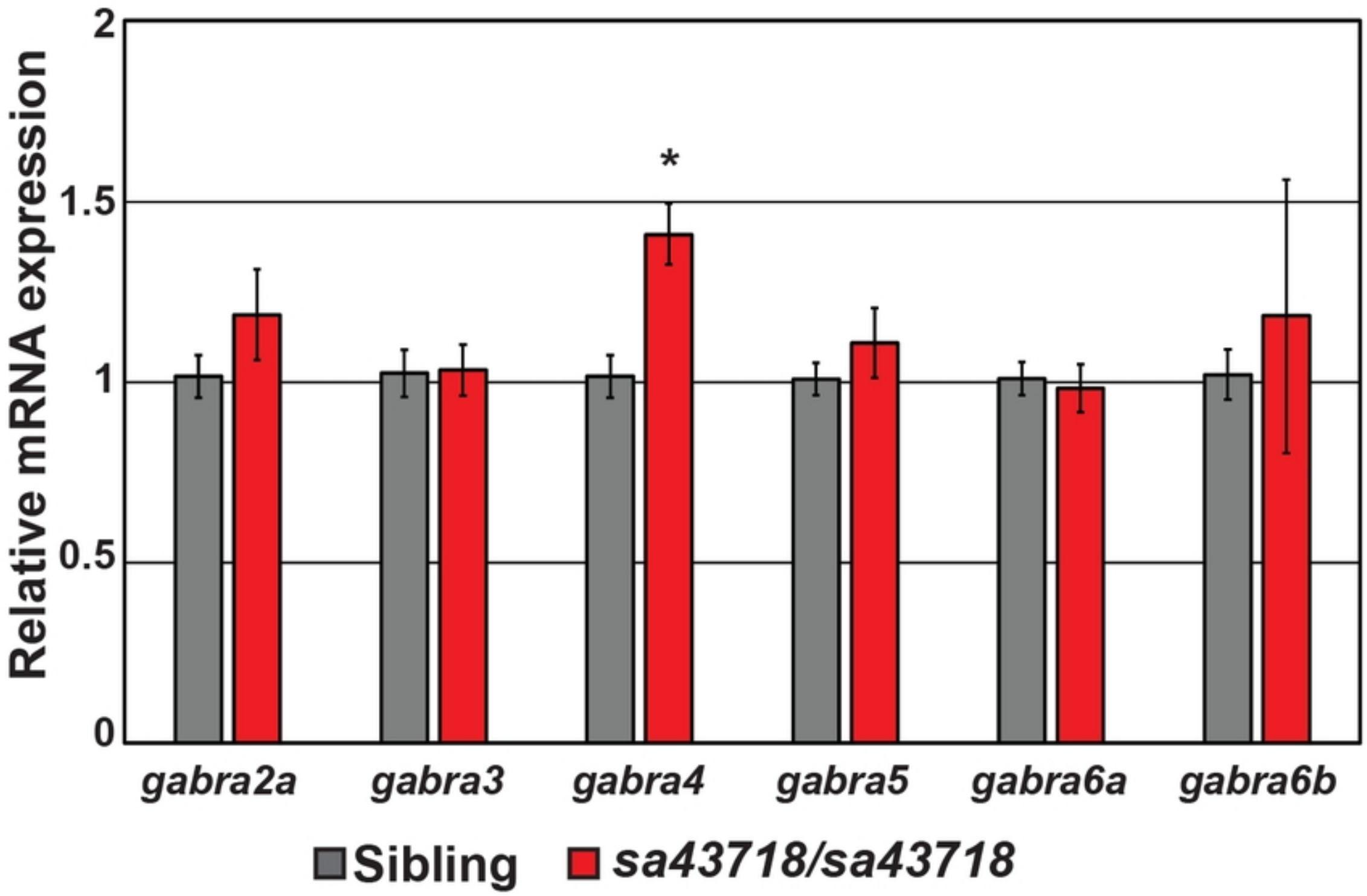
Relative mRNA expression
2
1.5
1
0.5
0
*
gabra2a
gabra3
gabra4
gabra5
gabra6a
gabra6b
Sibling
sa43718/sa43718

Figure 2

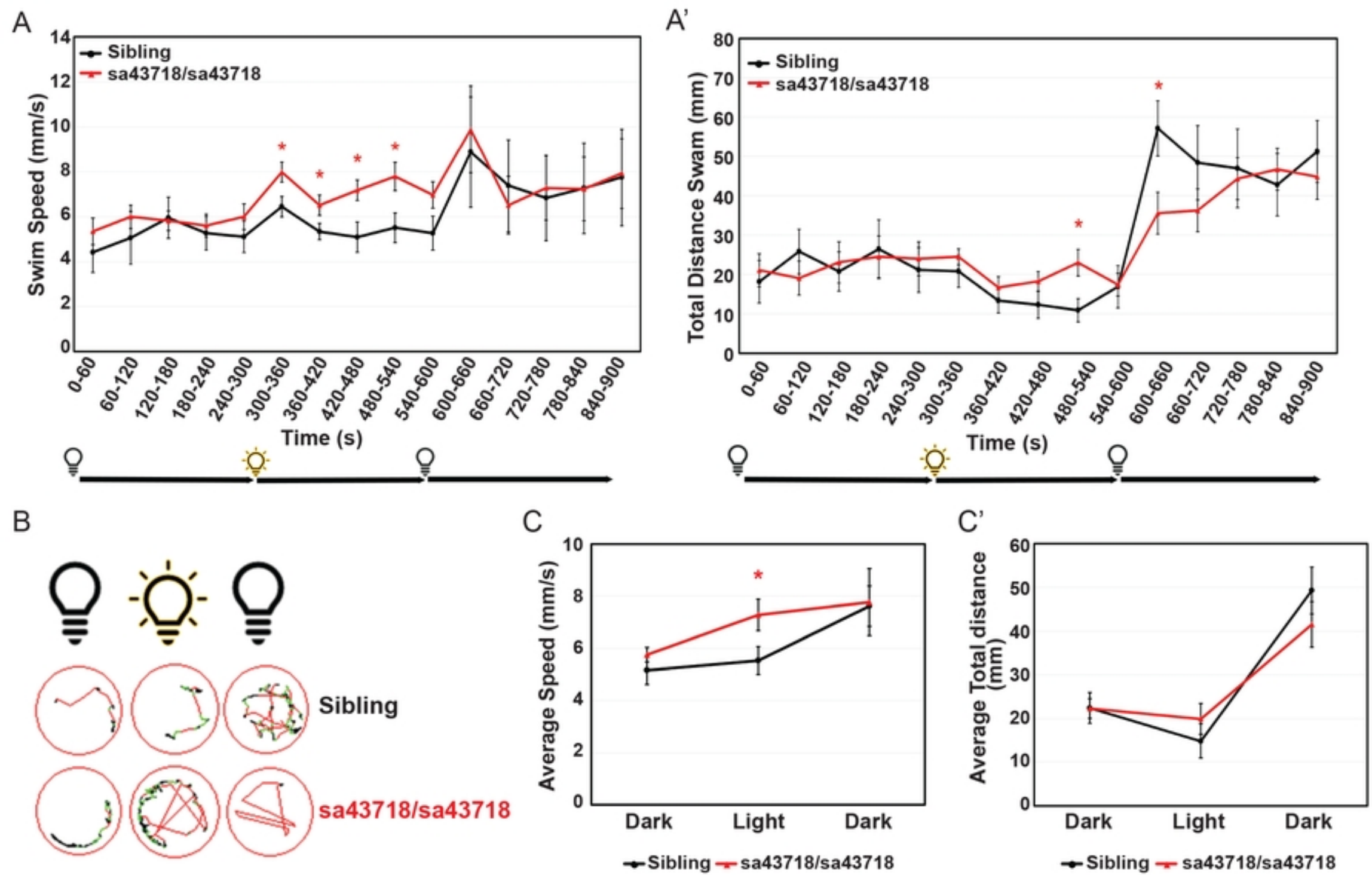
A
Sibling
sa43718/sa43718
Swim Speed (mm/s)
Time (s)
A'
Total Distance Swam (mm)
B
Sibling
sa43718/sa43718
C
Average Speed (mm/s)
Dark
Light
Dark
C'
Average Total distance (mm)

Figure 3

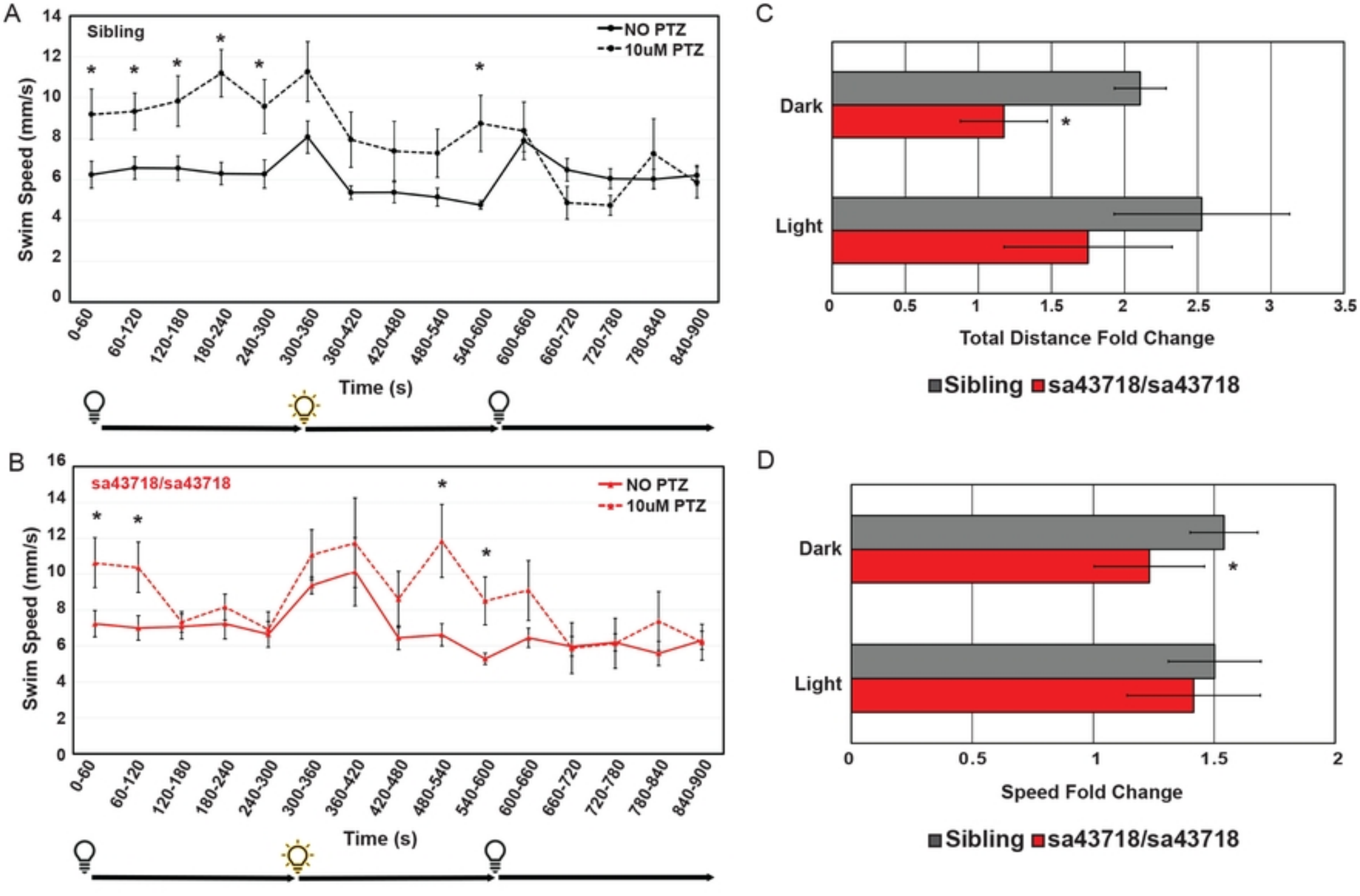
A
Sibling
NO PTZ
10uM PTZ
Swim Speed (mm/s)
Time (s)
0-60
60-120
120-180
180-240
240-300
300-360
360-420
420-480
480-540
540-600
600-660
660-720
720-780
780-840
840-900
B
sa43718/sa43718
NO PTZ
10uM PTZ
Swim Speed (mm/s)
Time (s)
C
Dark
Light
Total Distance Fold Change
Sibling
sa43718/sa43718
D
Dark
Light
Speed Fold Change
Sibling
sa43718/sa43718

Figure 4

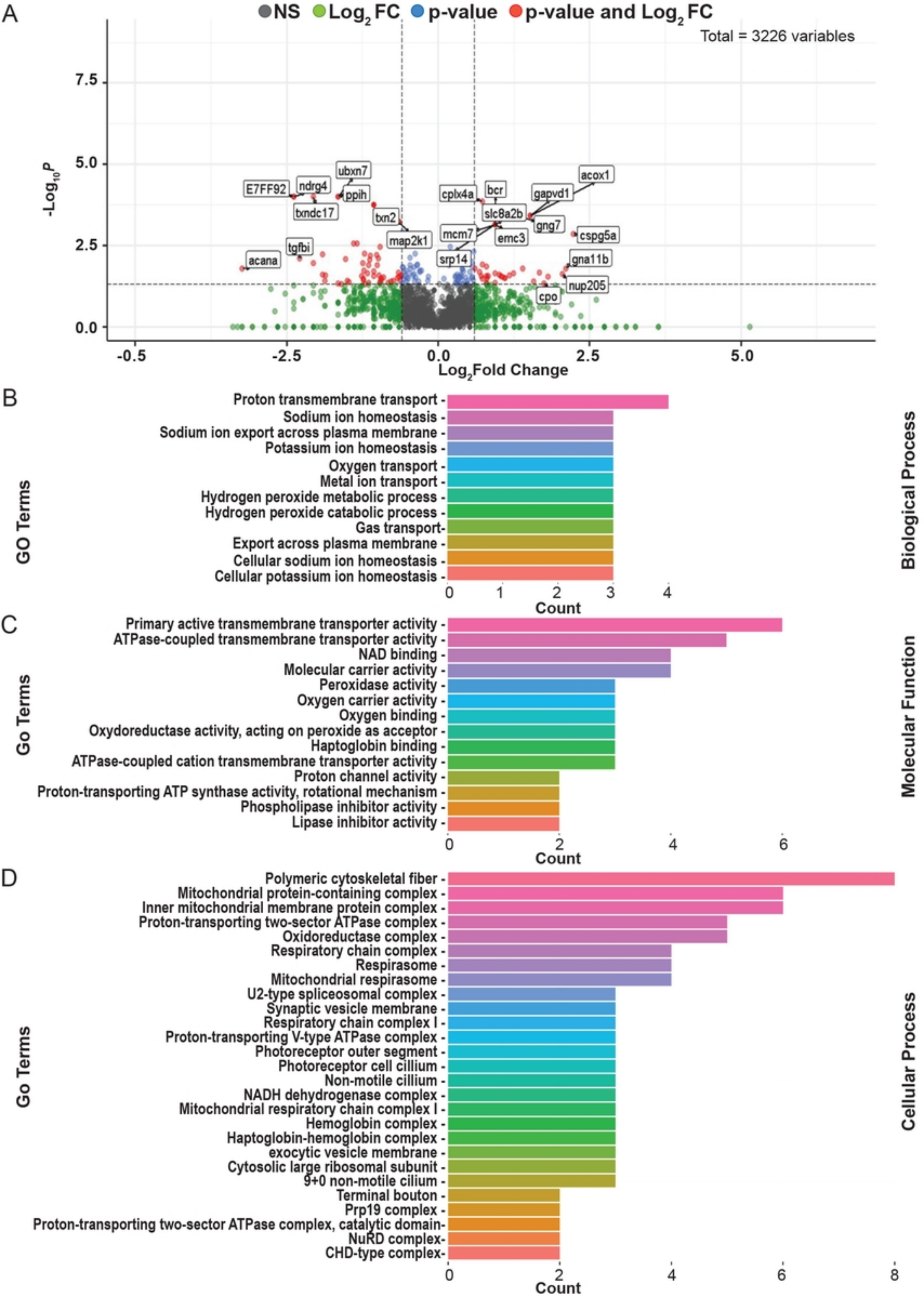
A
NS
Log2 FC
p-value
p-value and Log2 FC
Total = 3226 variables
-Log10P
Log2Fold Change
ubxn7
E7FF92
ndrg4
ppih
txndc17
txn2
map2k1
tgfbi
acana
cplx4a
bcr
slc8a2b
mcm7
emc3
srp14
gapvd1
acox1
gng7
cspg5a
gna11b
nup205
cpo
B
GO Terms
Proton transmembrane transport
Sodium ion homeostasis
Sodium ion export across plasma membrane
Potassium ion homeostasis
Oxygen transport
Metal ion transport
Hydrogen peroxide metabolic process
Hydrogen peroxide catabolic process
Gas transport
Export across plasma membrane
Cellular sodium ion homeostasis
Cellular potassium ion homeostasis
Count
Biological Process
C
Go Terms
Primary active transmembrane transporter activity
ATPase-coupled transmembrane transporter activity
NAD binding
Molecular carrier activity
Peroxidase activity
Oxygen carrier activity
Oxygen binding
Oxydoreductase activity, acting on peroxide as acceptor
Haptoglobin binding
ATPase-coupled cation transmembrane transporter activity
Proton channel activity
Proton-transporting ATP synthase activity, rotational mechanism
Phospholipase inhibitor activity
Lipase inhibitor activity
Count
Molecular Function
D
Go Terms
Polymeric cytoskeletal fiber
Mitochondrial protein-containing complex
Inner mitochondrial membrane protein complex
Proton-transporting two-sector ATPase complex
Oxidoreductase complex
Respiratory chain complex
Respirasome
Mitochondrial respirasome
U2-type spliceosomal complex
Synaptic vesicle membrane
Respiratory chain complex I
Proton-transporting V-type ATPase complex
Photoreceptor outer segment
Photoreceptor cell cillium
Non-motile cillium
NADH dehydrogenase complex
Mitochondrial respiratory chain complex I
Hemoglobin complex
Haptoglobin-hemoglobin complex
exocytic vesicle membrane
Cytosolic large ribosomal subunit
9+0 non-motile cilium
Terminal bouton
Prp19 complex
Proton-transporting two-sector ATPase complex, catalytic domain
NuRD complex
CHD-type complex
Count
Cellular Process

Figure 5